# Discretised Airy Stress Functions and Body Forces

Yu-Chou Chiang*, Pim Buskermolen, Andrew Borgart

Chair of Structural Design & Mechanics, Department of Architectural Engineering and Technology, Delft University of Technology
Julianalaan 134, 2628BL Delft, the Netherlands

* Corresponding author e-mail: Chiang.YuChou@gmail.com

## Abstract

*This paper extends polyhedral Airy stress functions to incorporate body forces. Stresses of an equilibrium state of a 2D structure can be represented by the second derivatives of a smooth Airy stress function and the integrals of body forces. In the absence of body forces, a smooth Airy stress function can be discretised into a polyhedron as the corresponding structure is discretised into a truss. The difference in slope across a creases represents the axial force on the bar, while the zero curvatures of the planar faces represent zero stresses voids of the structure. When body forces are present, the zero-stress condition requires the discretised Airy stress function to curve with the integrals of these body forces. Meanwhile, the isotropic angles on the creases still indicate concentrated axial forces. This paper discretises the integrals of body forces into step-wise functions, and discretises the Airy stress function into quadric faces connected by curved creases. The proposed method could provide structural designers (e.g. architects, structural engineers) with a more intuitive way to perceive stress fields.*

**Keywords:** Architectural geometry, Reciprocal force polygons, Isotropic geometry, Static equilibrium

# 1 Introduction

Statics is tightly bound with geometry by the works of Airy and Maxwell. Equilibrium states of two-dimensional structures can be represented by a scalar function, known as the Airy stress function (Sokolnikoff 1956). Airy (1863) suggested that the second derivatives of the function (or curvatures of the graph in isotropic geometry (see Pottmann and Opitz 1994; Chen et al. 2014)) can be regarded as stresses that automatically reach equilibrium states. A year after Airy's publication, Maxwell (1864) published a work seemingly independent to Airy's. It is also on statics, but concerns forces in trusses instead of stresses in continuous materials. Maxwell suggested the equilibrium of nodes in a truss be represented by force polygons, so that the collection of force polygons forms another truss-like figure. The original figure and the derived figure share a mutual relationship; they are reciprocal. Maxwell (1868, 1870) later suggested that when Airy's stress function is discretised into a polyhedron, that polyhedron has a reciprocal polyhedron of its own. The projections of the two polyhedrons are the reciprocal figures that he had introduced in Maxwell (1864). The axial forces in the bars of trusses are represented by the slope differences of the faces in the corresponding polyhedral Airy stress functions. The works of Airy and Maxwell have influenced further developments from hand-drawn graphic statics (Cremona 1890) to the latest computational statics (Fraternali et al. 2002; Block and Ochsendorf 2007).

Previous applications of discretised Airy stress functions only focus on external loads and ignore body forces. For a beam supporting a floor, the body forces from self-weight may indeed be negligible. However, for certain structures, such as rammed earth walls and flying buttresses, the self-weight may be the dominant load source.

This paper proposes using the curvature of the faces to represent body forces in discretised Airy stress functions. Curvature of the faces represents *in-active* stresses that become active body forces on the border between faces.

The remainder of this paper is organised as follows:

- **Section 2** discusses body forces in Airy stress functions and provides explanations through analytical methods and through the use of graphic statics.
- **Section 3** proposes the use of principal meshes (i.e. i-circular and i-conical meshes) with curved faces to discretise Airy stress functions and introduces them in Maxwell's reciprocal diagram.
- **Section 4** discusses the equilibrium at the boundaries (to complement the equilibrium inside the domain as discussed in the previous sections) .

- **Section 5** exhibits examples of simply supported beams.
- **Section 6** summarises the findings and suggests a direction for future research.

## 2 Mathematical and graphical explanation

This section explains why the faces in a discretised Airy stress function are curved when body forces are present. Two separate explanations are provided: **sec. 2.1** and **2.2** give the first explanation, showing how body forces are considered with smooth Airy stress functions, then discussing how to discretise them. **Section 2.3** applies graphic statics to reproduce the same phenomenon.

### 2.1 Smooth Airy stress functions and body forces

Stress functions are a means to derive stress tensors from scalar function(s) that automatically meet equilibrium conditions (Sokolnikoff 1956). The stress tensor $\boldsymbol{\sigma}$ for two-dimensional structures is often denoted as

$$\boldsymbol{\sigma} = \begin{bmatrix} \sigma_{xx} & \sigma_{xy} \\ \sigma_{xy} & \sigma_{yy} \end{bmatrix}, \tag{1}$$

in which $\sigma_{xx}$ and $\sigma_{yy}$ indicate normal stresses and $\sigma_{xy}$ indicates shear stress. Then the equilibrium conditions in x- and y-directions can be respectively expressed as

$$\begin{aligned} \frac{\partial}{\partial x}\sigma_{xx} + \frac{\partial}{\partial y}\sigma_{xy} + p_x = 0, \\ \frac{\partial}{\partial x}\sigma_{xy} + \frac{\partial}{\partial y}\sigma_{yy} + p_y = 0, \end{aligned} \tag{2}$$

where $p_x$ and $p_y$ are the body forces per unit area in x- and y-directions. The conditions **eq. (2)** are automatically satisfied once we introduce a smooth function $F(x, y)$ and define the stresses with the second derivatives of $F(x, y)$ along with the integrals of body forces (Heyman 1977) as

$$\begin{bmatrix} \sigma_{xx} & \sigma_{xy} \\ \sigma_{xy} & \sigma_{yy} \end{bmatrix} = \begin{bmatrix} F_{,yy} - \int p_x dx & -F_{,xy} \\ -F_{,xy} & F_{,xx} - \int p_y dy \end{bmatrix}. \tag{3}$$

In the equation above, the subscripts starting with a comma pose an alternative notation for derivatives so that $F_{,xx} = \frac{\partial^2}{\partial x^2}F$, $F_{,xy} = \frac{\partial^2}{\partial xy}F$, and $F_{,yy} = \frac{\partial^2}{\partial y^2}F$. Among engineers the arbitrary scalar function $F(x, y)$ is generally known as the Airy stress function.

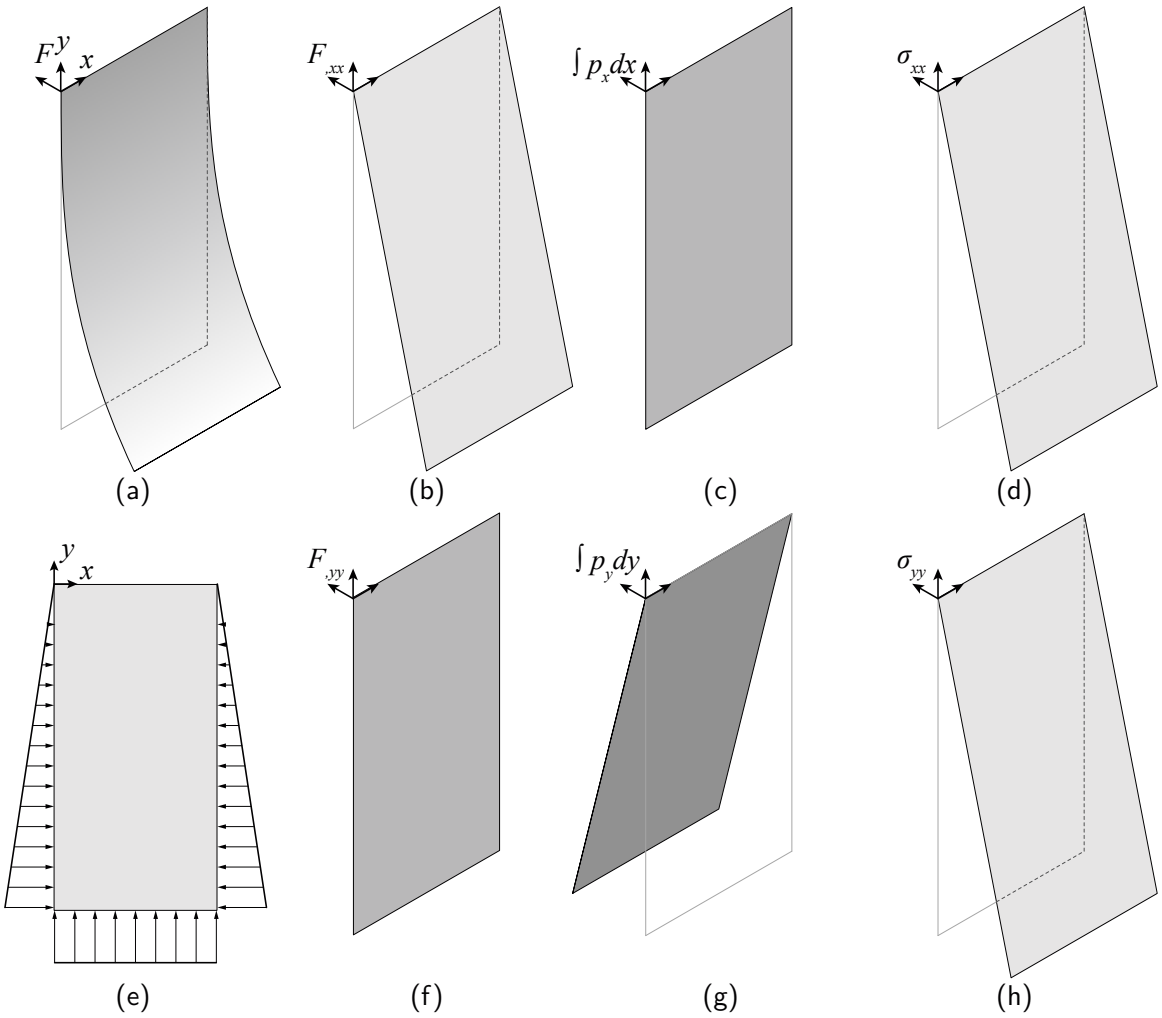


**Figure 1:** Hydrostatic pressure. (**a**) The Airy stress function. (**b-d**) The process of deriving the normal stress in x-direction. The second-derivative of the Airy stress function with respect to y (b), minus the integrals of the body forces in x (c) equals the stress in x-direction (d). (**f-h**) The process of deriving the normal stress in x-direction, equivalent to (b-d) but in perpendicular direction. (**e**) The stress distribution along the boundaries.

In the absence of body forces, the normal stress in x-direction $\sigma_{xx}$ is defined by the second derivative of the stress function with respect to the y-direction $F_{,yy}$. In the presence of body forces, only a portion of the second derivative should be regarded as the normal stress as the other part is covered (or rather subtracted) by $\int p_x \, dx$. The effects of $\int p_x \, dx$ and $\int p_y \, dy$ may initially not easily be recognised. A concrete example might help understand its application.

### Representing hydrostatic pressure.

Here we use the Airy stress function to represent a simple stress field. The pressure (or the stress) in a pool of static liquid is caused by the gravity, which is governed by $p_y = -\rho g$, in which $g$ is the gravitational load and $\rho$ is the fluid density. Since the fluid has no shear force capacity in any direction, we can say that $\sigma_{xy} = 0$ and

$\sigma_{xx} = \sigma_{yy}$. If we set $y = 0$ at the surface of the liquid, the stress should be:

$$\boldsymbol{\sigma}^{hydro} = \begin{bmatrix} \rho g y & 0 \\ 0 & \rho g y \end{bmatrix}. \tag{4}$$

We can set $\int p_x \, dx = 0$ and $\int p_y \, dy = -\rho g y$. Then, from **eq. (3)**, we can derive that $F^{hydro}_{,yy} = \rho g y$, $F^{hydro}_{,xx} = 0$. A sufficient solution to satisfy these conditions is

$$F^{hydro}(x, y) = \frac{1}{6} \rho g y^3. \tag{5}$$

**Figure 1** shows the spatial distribution of the stress function, its second-derivatives, integrals of body forces and the resulting stresses. Although this case is rather simple, we will see its "inner structure" once it is discretised.

## 2.2 Discretising Airy stress functions and the integrals of body forces

Different from stresses distributed across a continuous domain, discretised structures only have stresses concentrated in nodes and bars, and thus zero stresses in the voids (i.e. all of the space other than the nodes and bars). As the width of a bar approaches zero so that the stresses become highly concentrated, we tend to use axial force to refer to overall stress. The result is a substitute truss that approximates the original continuous structure. Body forces cannot be applied in the voids, as there are no structural members to transfer the load. Hence, we must apply the substitute loads (equivalent to the body forces) either on the nodes or the bars. In this example we choose bars to bear the body forces, which means we must discretise the integrals of body forces into step-wise functions. In every void, the $\int p_x \, dx$ and $\int p_y \, dy$ are constant. Loads in x-direction are resembled by the "stair risers" in $\int p_x \, dx$ between two adjacent voids. Loads in y-direction correspond to "stair risers" in $\int p_y \, dy$.

At the same time, the Airy stress function is also discretised into vertices, edges, and faces which correspond to the nodes, bars, and voids of the corresponding truss. Each face in the Airy stress function resembles a void bearing zero stress in the substitute structure. Hence, in the voids, the Airy stress function $F^{void}(x, y)$ should satisfy $\boldsymbol{\sigma}^{void} = \mathbf{0}$. Following from **eq. (3)**, we should have

$$\begin{aligned} F^{void}{}_{,yy} &= \int p_x \, dx \text{ and} \\ F^{void}{}_{,xx} &= \int p_y \, dy. \end{aligned} \tag{6}$$

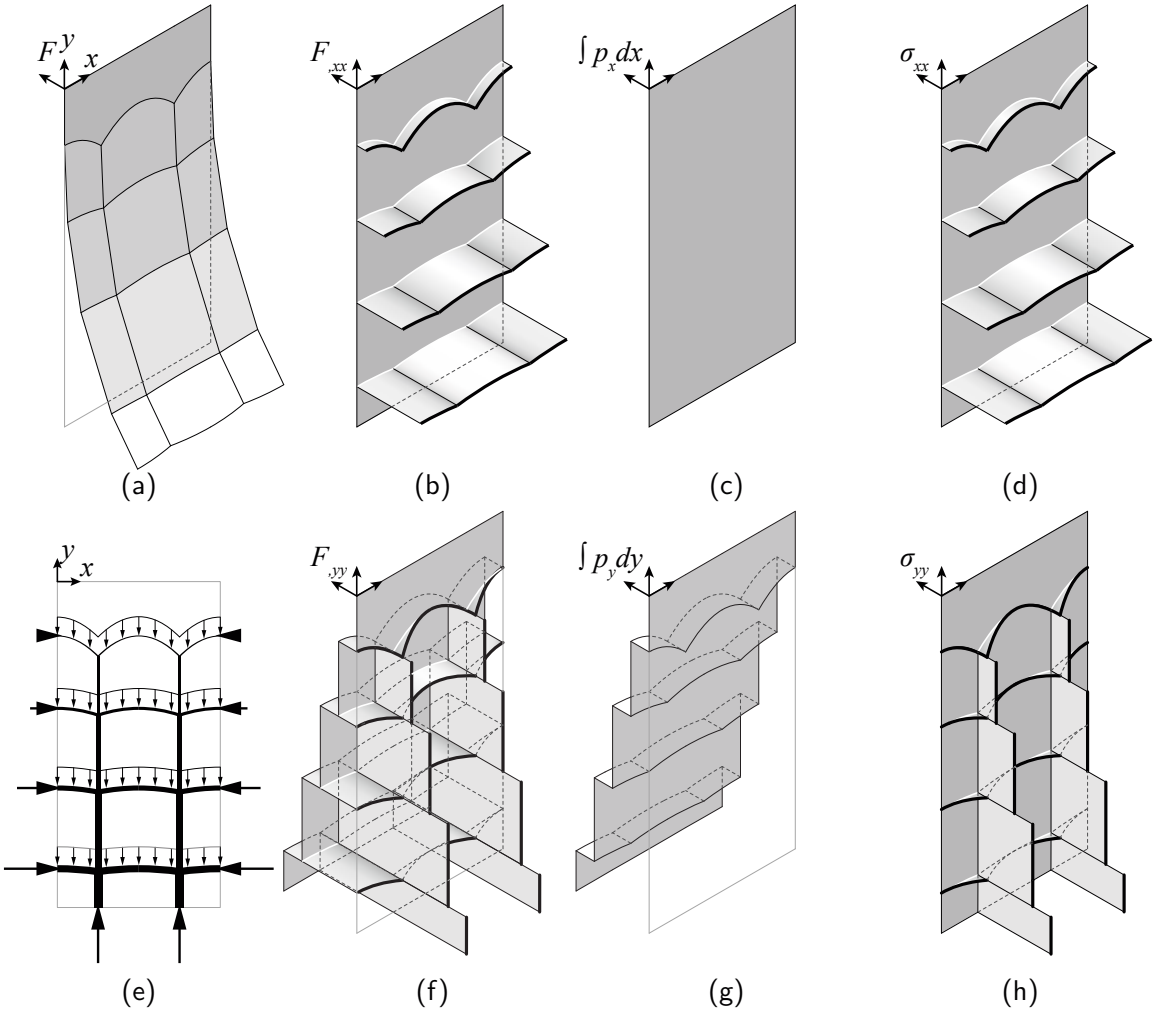


**Figure 2:** Discretised hydrostatic pressure. (**a**) The discretised Airy stress function, with curved faces and creases. (**b-d**) The derivation of the normal stress in x-direction. The second-derivative of the discretised Airy stress function with respect to y (b) minus the integrals of the body forces in x (c) equals the stress in x (d). (**f-h**) The derivation of the normal stress in y-direction, with the same process in (b-d). In panels (b, d, f, and h), the protruding surfaces ended by the black thick lines are a schematic representation of the Dirac delta function. The distance from the thick curve to the xy-plane is proportional to the crease angle of the stress function. (**e**) The structure approximating the hydrostatic pressure. The body forces turn into distributed loads on the *arches*, and the arches channel the loads into the *columns*. The arches at the lower level have larger horizontal forces thus have lower rises.

Since both $\int p_x \, dx$ and $\int p_y \, dy$ are constant in a void, $F^{void}$ should simply be a quadratic polynomial. Subsequently, the creases between these quadratic faces should be quadratic curves. It must be noted that the second derivatives at the creases are extremely intense, or more precisely, approach infinity. However, the integrals of such second derivatives are still a finite number, which can be interpreted as the slope differences across the creases. The differences between slopes represent the axial forces of the corresponding bars. As the second derivatives and the stresses approach infinity, we can use the Dirac delta function (Arfken et al. 2013, p. 75) to represent them.

**Discretising hydrostatic pressure.**

We use grid points $\mathbf{x}_{ij}$ to construct the Airy stress function in the voids $F_{ij}^{void}$. Grid points are given by

$$\mathbf{x}_{ij} = (\delta \cdot i, \delta \cdot j),$$

where $\delta$ is the spacing and $i, j$ are the indices such that $i \in \mathbf{Z}$, $j \in \{0, -1, -2, \cdots\}$. $F_{ij}^{void}$ is defined as polynomials that satisfy **eq. (6)** and is tangent to the smooth Airy stress function given in **eq. (5)**, at $\mathbf{x}_{ij}$. Such $F_{ij}^{void}$ can be expressed as

$$F_{ij}^{void} = \rho g \left( \frac{1}{6}\delta^3 j^3 + \frac{1}{2}\delta^2 j^2 (y - \delta j) - \frac{1}{2}\delta j (x - \delta i)^2 \right).$$

Each $F_{ij}^{void}$ intersects with its adjacent faces. The intersection of two faces defines a curved bar; an intersection of bars define a node. **Figure 2** shows the result of the discretised stress function. **Figure 2e** shows the *inter-structure* of hydrostatic pressure. The thrust of the arch increases with the depth and thus the raise decreases, while the column increases in thickness.

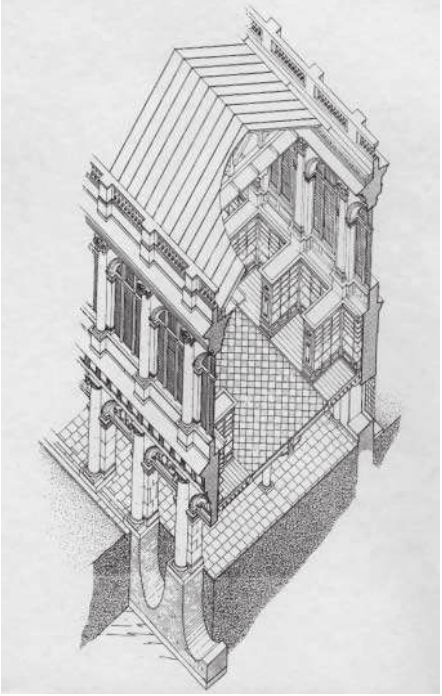

The proposed discretisation method does not invent the structure but rather discovers the nature of it. Similar structures had been discovered by architects centuries ago. **Figure 3** displays how Christopher Wren managed to use the inverted arch and horizontal thrust to collect vertical support from an area of earth to the columns.

**Figure 3:** The inverted arches as the foundations of Wren's Library for Trinity College, Cambridge (McKitterick 1995). [Used with permission from Cambridge University Press.]

## 2.3 Graphics statics and "in-active" forces

Graphic statics is primarily used to analyse the forces in a truss-like structure, first developed by Varignon (1725), and later developed by Maxwell (1864), Culmann (1866), and Cremona (1875)). A classical demonstration of graphic statics is given by the analysis of a cable's shape by hanging several weights as **fig. 4a** shows. The form diagram shows the cable deformed due to three weights, and the closed *force polygons* indicate that each node is in equilibrium.

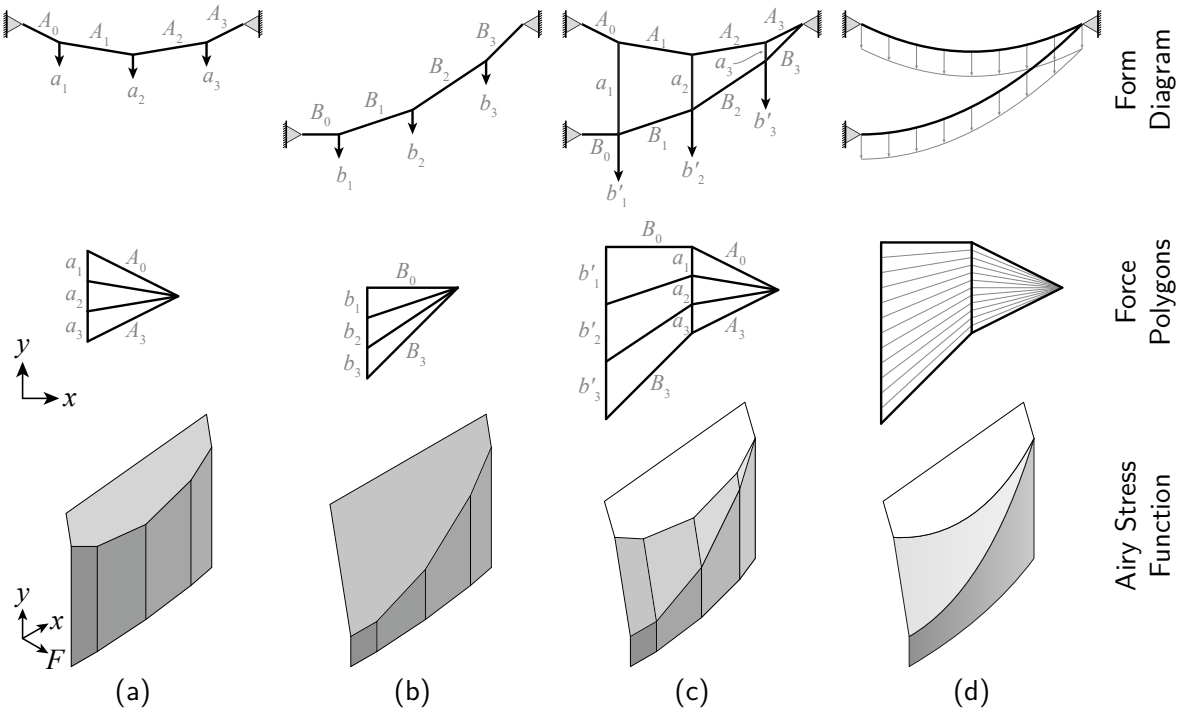


**Figure 4:** Hanging-chain models with corresponding force polygons and Airy stress functions. (**a**) A chain supporting three weights and anchored at levelled supports. (**b**) Another chain anchored at differing heights. (**c**) Two hanging chains in the same vertical plane. (**d**) Two chains with evenly distributed loads.

If another cable (**fig. 4b**) hangs right below the previous one, we can create aggregate force polygons (**fig. 4c**). The force polygons corresponding to the lower chain in **fig. 4c** show that it is not the absolute magnitude of the applied load $b'_i$ determining the shape of the lower chain, but that the shape is determined by the difference between the axial forces in $a_i$ and $b'_i$. Part of $b'_i$ is passing the lower chain and only the part of $b'_i - a_i$ is interacting with the lower chain. **Figure 4d** shows the force polygon when the loads are no longer applied at only three points, but all along the chain, as if they were distributed.

Regarding the airy stress functions in figure 4, the function in (c) has vertical edges to represent the loads of $a_i$ and $b'_i$. The stress function in (d) has smooth cylindrical surfaces with countless straight lines to represent distributed loads. One might notice that the stress function in (c) is actually the summation of the stress functions in (a) and (b).

# 3 Reciprocal diagrams and principal meshes in isotropic geometry

## 3.1 Maxwell's reciprocal diagrams

Maxwell (1868) proposed a mapping between two functions, $F(x, y)$ and $\phi(\xi, \eta)$:

$$\begin{aligned} \xi &= \frac{\partial F}{\partial x}, \quad \eta = \frac{\partial F}{\partial y}, \quad \phi = x\frac{\partial F}{\partial x} + y\frac{\partial F}{\partial y} - F, \\ x &= \frac{\partial \phi}{\partial \xi}, \quad y = \frac{\partial \phi}{\partial \eta}, \quad F = \xi\frac{\partial \phi}{\partial \xi} + \eta\frac{\partial \phi}{\partial \eta} - \phi. \end{aligned} \tag{7}$$

When $F(x, y)$ and $\phi(\xi, \eta)$ are smoothly differentiable, a point on $F(x, y)$ maps to another point on $\phi(\xi, \eta)$, and vice versa, thus Maxwell classified them as reciprocal diagrams.

Before explaining how a polygon maps to a vertex in conventional polyhedral Airy stress functions, we must first investigate the connection between the mapping and the second derivatives.

First, we conduct eigendecomposition on the Hessian matrix $\mathbf{H}^F$, and use eigenvalues to determine whether a point is on a vertex, an edge, or a planar face. The decomposition goes as follows:

$$\mathbf{H}^F = \begin{bmatrix} F_{,xx} & F_{,xy} \\ F_{,xy} & F_{,yy} \end{bmatrix} = \mathbf{Q}\begin{bmatrix} \lambda_1^F & 0 \\ 0 & \lambda_2^F \end{bmatrix}\mathbf{Q}^{-1}, \tag{8}$$

in which $\mathbf{Q}$ is a $2 \times 2$ orthogonal matrix formed by the eigenvectors, and $\lambda_1^F$ and $\lambda_2^F$ are the eigenvalues. We can say a region is planar when the local $\lambda_1^F = \lambda_2^F = 0$, a point is on an edge when one of the eigenvalues equals 0 and the other has infinite magnitude, and a point is on a vertex if $|\lambda_1^F| = |\lambda_2^F| = \infty$.

How a group of surrounding points on $F(x, y)$ maps to $\phi(\xi, \eta)$, can be described by a Jacobian matrix as

$$\mathbf{J}_{(x,y)\to(\xi,\eta)} = \begin{bmatrix} \xi_{,x} & \xi_{,y} \\ \eta_{,x} & \eta_{,y} \end{bmatrix}.$$

From **eq. (7)**, we can derive

$$\mathbf{J}_{(x,y)\to(\xi,\eta)} = \begin{bmatrix} F_{,xx} & F_{,xy} \\ F_{,xy} & F_{,yy} \end{bmatrix}. \tag{9}$$

One might notice that the right hand side of **eq. (9)** is also the Hessian matrix of $F(x, y)$. The inverse mapping can also be described by another Jacobian matrix, which would be the inverse matrix of the Jacobian in the forward mapping (Arfken et al. 2013, p. 230):

$$\mathbf{J}_{(\xi,\eta)\to(x,y)} = \left[\mathbf{J}_{(x,y)\to(\xi,\eta)}\right]^{-1}. \tag{10}$$

The inverse Jacobian matrix should also be the Hessian matrix on $\phi(\xi,\eta)$. Combining **eq. (10)** with **eq. (8)** and **(9)**, we can say that

$$\mathbf{J}_{(\xi,\eta)\to(x,y)} = \left[\mathbf{H}^F\right]^{-1} = \mathbf{Q}\begin{bmatrix} \frac{1}{\lambda_1^F} & 0 \\ 0 & \frac{1}{\lambda_2^F} \end{bmatrix}\mathbf{Q}^{-1} = \mathbf{Q}\begin{bmatrix} \lambda_1^\phi & 0 \\ 0 & \lambda_2^\phi \end{bmatrix}\mathbf{Q}^{-1} = \mathbf{H}^\phi, \quad (11)$$

where $\mathbf{H}^\phi$ is the Hessian matrix corresponding to $\mathbf{H}^F$, and $\lambda_1^\phi$ and $\lambda_2^\phi$ are the eigenvalues corresponding to $\lambda_1^F$ and $\lambda_2^F$. **Equation (11)** suggests an interesting relation between $F(x,y)$ and $\phi(\xi,\eta)$:

- a point on $F(x,y)$ has the same set of eigenvectors $\mathbf{Q}$ as the corresponding point on $\phi(\xi,\eta)$, and
- the eigenvalues $\lambda_1^F$ and $\lambda_2^F$ on $F(x,y)$ are the reciprocal numbers (or multiplicative inverses) of the corresponding eigenvalues $\lambda_1^F$ and $\lambda_2^F$ on $\phi(\xi,\eta)$.

**Table 1** classifies the types of geometric entities by the magnitudes of their eigenvalues and shows for each entity its corresponding reciprocal entity. **Figure 5** shows how this translates into geometric relations between $F(x,y)$ and $\phi(\xi,\eta)$.

| **Entity in** $F(x,y)$ | $\lvert\lambda_1^F\rvert$ | $\lvert\lambda_2^F\rvert$ | **Entity in** $\phi(\xi,\eta)$ | $\lvert\lambda_1^\phi\rvert$ | $\lvert\lambda_2^\phi\rvert$ |
|---|---|---|---|---|---|
| Vertex | $\infty$ | $\infty$ | Planar surf. | $0$ | $0$ |
| Curved edge | $0\cdots\infty$ | $\infty$ | Developable surf. | $0\cdots\infty$ | $0$ |
| Straight edge | $0$ | $\infty$ | Straight edge | $\infty$ | $0$ |
| Doubly curved surf. | $0\cdots\infty$ | $0\cdots\infty$ | Doubly curved surf. | $0\cdots\infty$ | $0\cdots\infty$ |
| Developable surf. | $0$ | $0\cdots\infty$ | Curved edge | $\infty$ | $0\cdots\infty$ |
| Planar surf. | $0$ | $0$ | Vertex | $\infty$ | $\infty$ |

**Table 1:** Reciprocal relations between geometric entities.

## 3.2 Isotropic geometry

Isotropic geometry refers to an $n$-variable scalar function in an $(n+1)$-dimensional space (Pottmann and Opitz 1994; Pottmann and Liu 2007; Chen et al. 2014). This way, a 2D scalar function $f : D \subset \mathbf{R}^2 \to \mathbf{R}$ defined on a domain $D$ becomes a 3D surface

$$\Big\{(x,y,f(x,y)) \in \mathbf{R}^3 : (x,y) \in D\Big\}.$$

Subsequently, we can discuss functions from a geometric point of view such that gradients of a function relate to slopes in a surface, and the second derivatives relate to normal curvatures. Since the third dimension is different from the other two, isotropic geometry treats this last dimension distinctively.

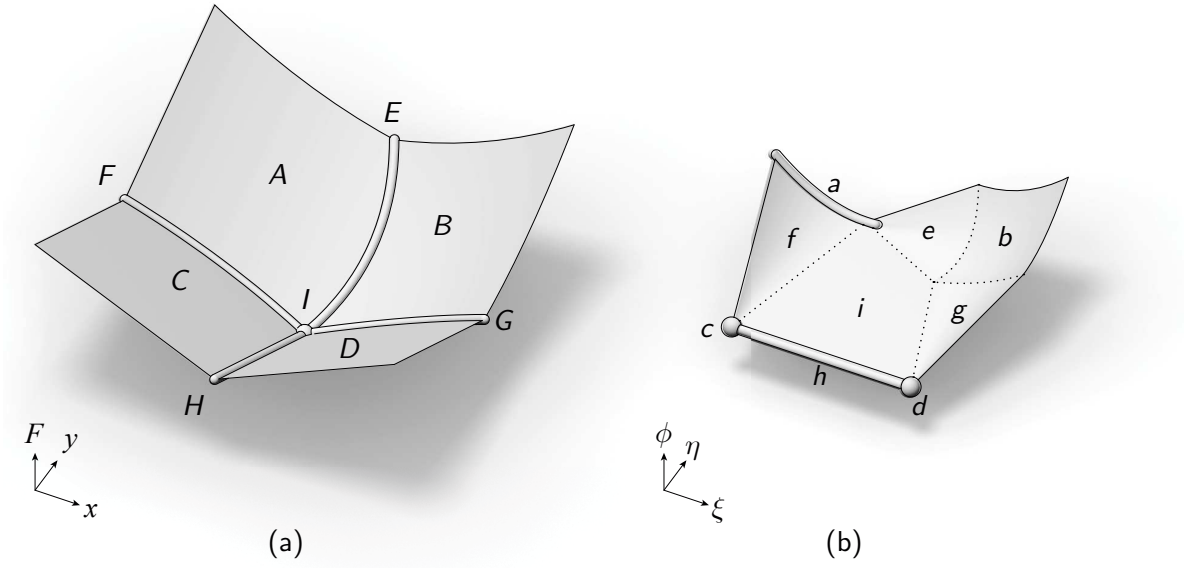


**Figure 5:** A pair of reciprocal diagrams. (**a**) the left diagram consists of four surfaces (A: developable, B: doubly curved, C-D: planar), four edges (E-G: curved, H: straight), and one vertex (I). (**b**) The corresponding entities are labelled in lowercase letters. Surfaces b, e, f, g, and i have continuous slope; The borders between surfaces A, B, C, and D have crease angles.

We can plot the Airy stress function as a surface in the 3D space and apply principal meshes to visualise and discretise the Airy stress "surface". Principal meshes are quad-dominant meshes which can effectively reveal principal curvatures of surfaces (Liu et al. 2006; Zadravec et al. 2010). Since the normal curvatures on the Airy stress surfaces are the second-derivatives that indicate stresses, principal meshes ultimately display the principal stresses. As the third dimension of the Airy stress surfaces is not a physical dimension, we opt to apply their counterparts in isotropic geometry, *isotropic*-circular and *isotropic*-conical meshes (from here on referred to as *i*-circular and *i*-conical meshes respectively).

In isotropic geometry, the notions of distance, circle, and sphere differ from their Euclidean counterparts. For detailed definitions, see Pottmann and Opitz (1994); Pottmann and Liu (2007). Here we briefly mention the notions that are crucial in *i*-circular and *i*-conical meshes.

### *Isotropic*-distance.

The major distinction of 3D isotropic geometry from the ordinary 3D Euclidean geometry is that the first two dimensions are more important than the last. The *i*-distance between two points $\mathbf{x}_1 = (x_1, y_1, z_1)$ and $\mathbf{x}_2 = (x_2, y_2, z_2)$ is barely affected by the third dimension, such that

$$\|\mathbf{x}_1 - \mathbf{x}_2\|_i := \lim_{\epsilon \to 0} \sqrt{(x_1 - x_2)^2 + (y_1 - y_2)^2 + \epsilon^2 (z_1 - z_2)^2},$$

in which the third dimension is almost negligible as $\epsilon \to 0$.

***Isotropic*-sphere.**

Following from the definition of *i*-distance, the *i*-sphere is the set of all points $\mathbf{x} = (x, y, z)$ with a constant distance $r$ from a centre $\mathbf{x}_c$ such that $\|\mathbf{x} - \mathbf{x}_c\|_i = r$ or

$$(x - x_c)^2 + (y - y_c)^2 + \epsilon^2 (z - z_c)^2 = r^2.$$

When $0 < \epsilon^2 < 1$, the "sphere" looks like an ellipsoid obtained by rotating an ellipse about the z-axis, which has two foci. Let $(x_c, y_c, z_1^{focus})$ denote the higher focus and $(x_c, y_c, z_2^{focus})$ the lower. When $\epsilon \to 0$, the ellipsoid degenerates into a circular cylinder (as $z_1^{focus} \to \infty$ and $z_2^{focus} \to -\infty$), or a paraboloid of revolution (as one of $|z_1^{focus}|$ and $|z_2^{focus}|$ approaches infinity while the other stays finite). The former degenerated ellipsoid is the *i*-sphere of cylindrical type and the latter is the *i*-sphere of parabolic type. Thus the *i*-sphere of cylindrical type can be expressed as

$$(x - x_c)^2 + (y - y_c)^2 = r^2.$$

The *i*-sphere of parabolic type can be expressed as

$$(x - x_c)^2 + (y - y_c)^2 + c_1 z = c_2,$$

where $c_1$ and $c_2$ are constants that relate to $z_c$ and $r^2$. Thus the unit *i*-sphere of parabolic type $\Sigma_0$ is defined as

$$\Sigma_0 := \left\{ (x, y, \frac{1}{2}(x^2 + y^2)) : (x, y) \in \mathbf{R}^2 \right\}.$$

## 3.3 Reciprocity between planar *i*-circular and *i*-conical Meshes

Pottmann and Wallner (2008) describe that "Circular meshes are quadrilateral meshes all of whose faces possess a circumcircle, whereas conical meshes are planar quadrilateral meshes where the faces which meet in a vertex are tangent to a right circular cone [or a sphere]."

In isotropic geometry, the definition of spheres is changed. As a result, the definitions of *i*-circular meshes and *i*-conical meshes change too (Pottmann and Liu 2007). *I*-circular meshes refer to meshes where the vertices forming a face are on the intersection between a plane and an *i*-sphere; *i*-conical meshes refer to planar meshes where the faces meeting in a vertex are tangent to an *i*-sphere.

An *i*-circular mesh inscribed in the unit *i*-sphere $\Sigma_0$ is reciprocal to an *i*-conical mesh circumscribed about the unit *i*-sphere $\Sigma_0$ (Pottmann and Liu 2007). We will extend this notion and show that an *i*-circular mesh inscribed in a surface $(x, y, F(x, y))$ is reciprocal to an *i*-conical mesh circumscribed about the reciprocal surface $(\xi, \eta, \phi(\xi, \eta))$ defined in **eq. (7)**. The notion consists of two steps:

1. Planes tangent to $(\xi, \eta, \phi(\xi, \eta))$ at points $(\xi_i, \eta_i, \phi_i)$ meet at one vertex if and only if the corresponding points $(x_i, y_i, F_i)$ are on a plane.
2. Planes tangent to $(\xi, \eta, \phi(\xi, \eta))$ at points $(\xi_i, \eta_i, \phi_i)$ are tangent to an *i*-sphere if and only if the corresponding points $(x_i, y_i, F_i)$ are on an *i*-sphere.

In the first step, let $(\xi_i, \eta_i, \phi_i)$ denote 3 distinctive points, in which $i \in \{1, 2, 3\}$, and $(x_i, y_i, F_i)$ denote the corresponding points. A plane tangent to $(\xi, \eta, \phi(\xi, \eta))$ at $(\xi_i, \eta_i, \phi_i)$ can be expressed as

$$\zeta = \phi_i + \phi_{,\xi}(\xi_i, \eta_i) \cdot (\xi - \xi_i) + \phi_{,\eta}(\xi_i, \eta_i) \cdot (\eta - \eta_i).$$

From **eq. (7)**, we can rewrite the tangent plane as

$$\zeta = x_i \cdot \xi + y_i \cdot \eta - F_i. \tag{12}$$

Let $(\xi_v, \eta_v, \zeta_v)$ denote the intersection of the three tangent planes defined by the three points. The intersection $(\xi_v, \eta_v, \zeta_v)$ is provided by

$$\begin{bmatrix} \xi_v \\ \eta_v \\ \zeta_v \end{bmatrix} = \begin{bmatrix} x_1 & y_1 & -1 \\ x_2 & y_2 & -1 \\ x_3 & y_3 & -1 \end{bmatrix}^{-1} \begin{bmatrix} F_1 \\ F_2 \\ F_3 \end{bmatrix} \tag{13}$$

Any non-vertical plane that passes through $(\xi_v, \eta_v, \zeta_v)$ and is tangent to $(\xi, \eta, \phi(\xi, \eta))$ at points $(\xi_t, \eta_t, \phi_t)$ should meet the condition:

$$\zeta_v = x_t \cdot \xi_v + y_t \cdot \eta_v - F_t, \tag{14}$$

where $(x_t, y_t, F_t)$ is the point corresponding to $(\xi_t, \eta_t, \phi_t)$. **eq. (14)** describes the valid point of tangency $(x_t, y_t, F_t)$ on a plane of $F_t = \xi_v \cdot x_t + \eta_v \cdot y_t - \zeta_v$ in $(x, y, F(x, y))$ as **fig. 6** shows. It should be noted that this plane also passes through the three points found with **eq. (13)**.

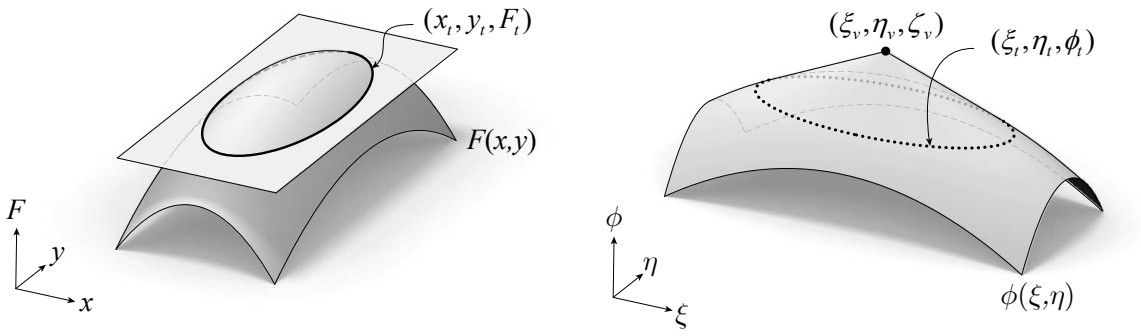


**Figure 6:** The intersection of a plane with $F(x, y)$ defines $(x_t, y_t, F_t)$, which corresponds to a set of tangency points $(\xi_t, \eta_t, \phi_t)$ that define planes passing through $(\xi_v, \eta_v, \zeta_v)$.

In the second step, we consider the reciprocal diagrams of $(x, y, F(x, y))$ and $(\xi, \eta, \phi(\xi, \eta))$ along with *i*-spheres. Let $S$ denote an *i*-sphere of hyperbolic type

$$S = \left\{ \left( x, y, \frac{a}{2}\left((x-x_s)^2 + (y-y_s)^2\right) + z_s \right) : (x,y) \in \mathbf{R}^2 \right\}.$$

Each *i*-spheres $S$ has four parameters: $a$, $x_s$, $x_s$, and $z_s$. Let $\Sigma$ denote the corresponding *i*-sphere of $S$. By **eq. (7)**, we can derive

$$\Sigma = \left\{ \left( \xi, \eta, \frac{1}{2a}\left((\xi + ax_s)^2 + (\eta + ay_s)^2\right) - z_s - \frac{a}{2}(x_s^2 + y_s^2) \right) : (\xi,\eta) \in \mathbf{R}^2 \right\}.$$

If the *i*-sphere $\Sigma$ is inscribed by the planes from **eq. (12)**, the slopes of the graphs should match at the points of tangency $(\xi_{\Sigma_i}, \eta_{\Sigma_i}, \zeta_{\Sigma_i})$. For the slope in x-direction, we have

$$\begin{aligned} &\frac{\partial}{\partial \xi}(x_i \cdot \xi + y_i \cdot \eta - F_i)\Big|_{\xi=\xi_{\Sigma_i}, \eta=\eta_{\Sigma_i}} \\ &\qquad = \frac{\partial}{\partial \xi}\left( \frac{1}{2a}\left((\xi + ax_s)^2 + (\eta + ay_s)^2\right) - z_s - \frac{a}{2}(x_s^2 + y_s^2) \right)\Big|_{\xi=\xi_{\Sigma_i}, \eta=\eta_{\Sigma_i}}, \end{aligned}$$

which gives us

$$\xi_{\Sigma_i} = a(x_i - x_s).$$

In the same manner, the condition in y-direction gives $\eta_{\Sigma_i} = a(y_i - y_s)$. When we project $(\xi_{\Sigma_i}, \eta_{\Sigma_i})$ vertically to the tangent plane and $\Sigma$, the two results should be equal, so that

$$ax_i \cdot (x_i - x_s) + ay_i \cdot (y_i - y_s) - F_i = \frac{a}{2}(x_i^2 + y_i^2) - z_s - \frac{a}{2}(x_s^2 + y_s^2),$$

which is equivalent to

$$F_i = \frac{a}{2}\left((x_i - x_s)^2 + (y_i - y_s)^2\right) + z_s. \tag{15}$$

**Equation (15)** suggests that if the unit *i*-sphere $\Sigma$ is inscribed in the tangent planes defined by $\boldsymbol{\xi}_i = (\xi_i, \eta_i, \phi_i)$, the corresponding *i*-sphere $S$ is circumscribed about the corresponding points $\mathbf{x}_i = (x_i, y_i, F_i)$.

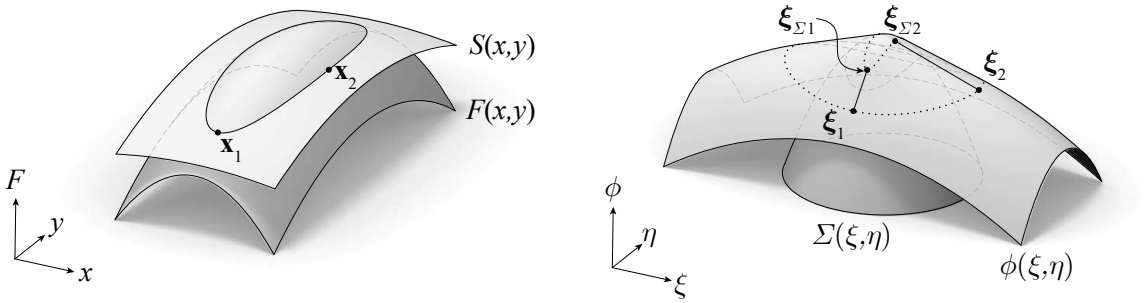


**Figure 7:** Points on the intersection of $F(x, y)$ and $S(x, y)$ correspond to lines tangent to both $\phi(\xi, \eta)$ and $\Sigma(\xi, \eta)$ at $\boldsymbol{\xi}_i$ and $\boldsymbol{\xi}_{\Sigma_i}$ respectively. Two instances of the tangent lines are explicitly drawn.

A vertex $(x_i, y_i, F_i)$ on $F(x, y)$ is reciprocal to a plane tangent to $\phi(\xi, \eta)$ at the corresponding points $(\xi_i, \eta_i, \phi_i)$. Considering **eq. (14)** and **(15)**, we can say that when $(x_i, y_i, F_i)$ is a set of *i*-concyclic vertices, the reciprocal planes meet at one point and are circumscribed about an *i*-sphere. Thus, an *i*-circular mesh inscribed in $F(x, y)$ corresponds to an *i*-conical mesh that is circumscribed about $\phi(\xi, \eta)$.

## 3.4 *I*-circular and *i*-conical Airy stress functions with discretised body forces

When body forces are introduced, the discretised Airy stress function should have curved faces to meet the zero stress conditions stated in **eq. (6)**. Given that the existing definitions on *i*-circular and *i*-conical meshes are restricted to planar faces, we must propose generalised definitions for *i*-circular and *i*-conical meshes. Non-planar *i*-circular meshes are quadrilateral meshes that the vertices of each face are on an *i*-sphere of cylindrical type. Non-planar *i*-conical meshes are quadrilateral meshes that the surround faces of each vertex are tangent to lateral faces of a pyramid at the apex, and the pyramid is circumscribed about an *i*-sphere of parabolic type.

**Figure 8** shows a set of points $\mathbf{x}_i$ that are on the intersection of an *i*-sphere of cylindrical type $S$, the graph of the local zero-stress stress function $F^{void}$, and the smooth stress function $F$.

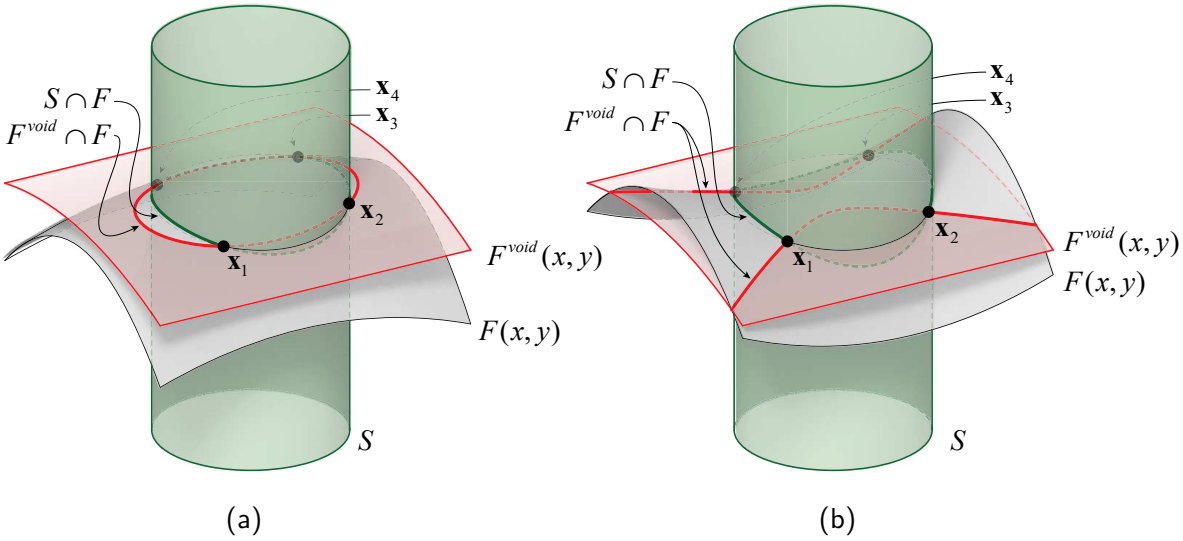


**Figure 8:** Points $\mathbf{x}_i$ on the intersection of an *i*-sphere of cylindrical type $S$, the graph of the local zero-stress stress function $z = F^{void}(x, y)$, and the graph of the stress function $z = F(x, y)$. (**a**) A case in which $F$ has positive Gaussian curvature. (**b**) A case in which $F$ has negative Gaussian curvature.

Given a smooth Airy stress function $F(x, y)$, and integrals of body forces $P_x(x, y) = \int p_x \, dx$ and $P_y(x, y) = \int p_y \, dy$, we can find a non-planar *i*-circular mesh inscribed in the stress function $F$.

To start with the first face, we choose three of the points arbitrarily. The three points determine the centre $(x_c, y_c)$ and the radius of an *i*-sphere of cylindrical type $S$. We can use the values of $P_x(x_c, y_c)$ and $P_y(x_c, y_c)$ to determine the local value of step-wise functions $P_x^{disc}(x, y)$ and $P_y^{disc}(x, y)$ which are the discretised versions of $P_x(x, y)$ and $P_y(x, y)$. Subsequently, we can define $F^{void}$ in a polynomial form:

$$F^{void}(x, y) = \frac{P_y^{disc}(x_c, y_c)}{2} x^2 + \frac{P_x^{disc}(x_c, y_c)}{2} y^2 + ax + by + c, \qquad (16)$$

in which $a$, $b$, and $c$ are constants. **Equation (16)** is arranged in such a way to satisfy **eq. (6)**. The constants $a$, $b$, and $c$ can be determined by the three points. Thus we have fixed $S$ and $F^{void}$, the fourth point can be located at the intersection of $S$, $F$, and $F^{void}$. Here we can derive one point of a 2-by-2 mesh when three points are given. In regions with no umbilical point (Porteous 2001), we can derive a quadrilateral mesh with m-by-n points when m+n−1 points are given.

When $\int p_x \, dx$ and $\int p_y \, dy$ equal zero, all faces of $F^{void}(x, y)$ are planar, and a planar *i*-circular mesh can be derived. Moreover, a planar *i*-conical mesh circumscribed about $F(x, y)$ can also be derived by applying this method by discretising the reciprocal diagram $\phi(\xi, \eta)$ into an *i*-circular mesh first. Then the mesh can be mapped by **eq. (7)**, resulting in the *i*-conical mesh as discussed in **sec. 3.3**.

Regarding a non-planar *i*-conical mesh that circumscribes about a smooth graph of $F(x, y)$, an example on hydrostatic pressure was shown in **sec. 2.2**. In that example, each face of the discretised Airy stress function was constructed based on a grid point, so that the faces were constructed as

$$F^{void}(x, y|x_b, y_b) = \frac{P_y(x_b, y_b)}{2}(x - x_b)^2 + \frac{P_x(x_b, y_b)}{2}(y - y_b)^2 + F_{,x}(x_b, y_b)(x - x_b) + F_{,y}(x_b, y_b)(y - y_b) + F(x_b, y_b), \quad (17)$$

where $(x_b, y_b)$ is the base point. The curvatures of $F^{void}(x, y)$ are informed by $P_y(x, y)$ and $P_x(x, y)$ at the base point $(x_b, y_b)$, and the overall slope and elevation are determined such that $F^{void}(x, y)$ is tangent to $F(x, y)$ at the base point $(x_b, y_b)$.

We first discuss how four base points $\mathbf{x}_i = (x_i, y_i, z_i)$ can construct a set of $F_i^{void}(x, y)$ that meet in one point. Three of the graphs $F_i^{void}(x, y)$ can easily meet at one point, say $\mathbf{x}_v = (x_v, y_v, z_v)$. If the fourth face also passes the same point with correct slopes, then we can fulfil the criteria set in the first paragraph of this subsection. The passing through the point $\mathbf{x}_v$ is relatively easily expressed in an equation:

$$F_4^{void}(x_v, y_v|x_4, y_4) = z_v. \quad (18)$$

Regarding the slopes, one can approach $\mathbf{x}_v$ from different base points $\mathbf{x}_i$. The observed slope can be expressed as

$$\text{x component: } \xi_{vi} = F_{i,x}^{void}(x_v, y_v|x_i, y_i), \text{ and}$$
$$\text{y component: } \eta_{vi} = F_{i,y}^{void}(x_v, y_v|x_i, y_i).$$

Form Maxwell's point of view, the slopes $(\xi_{vi}, \eta_{vi})$ regard points in the reciprocal diagram, and the vertex $\mathbf{x}_v$ corresponds to the polygon formed by $(\xi_{vi}, \eta_{vi})$. Whenever the polygon is cyclic, the orientation of Planes tangent to $F_i^{void}$ at $\mathbf{x}_v$ will circumscribe an *i*-sphere, thus meet the criteria for *i*-conical meshes. The polygon is cyclic when the following equation is met:

$$(\xi_{vi} - \xi_c)^2 + (\eta_{vi} - \eta_c)^2 = \rho_c^2, \quad (19)$$

in which $(\xi_c, \eta_c)$ is the centre and $\rho_c$ is the radius of the circumscribe circle (see **fig. 9**). **Equations (18)** and **(19)** together can determine the legitimate fourth base point and make the vertex $\mathbf{x}_v$ meet the *i*-conical condition.

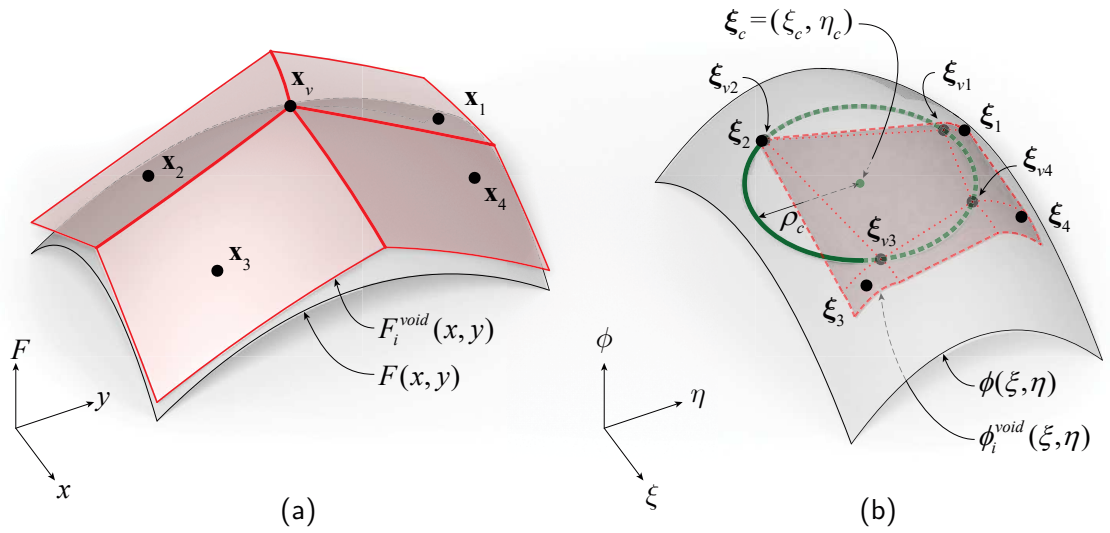


**Figure 9:** Reciprocal diagrams of the smooth stress function $F(x,y)$ and faces of the discretised stress function $F_i^{void}(x,y)$. The faces tangent to $F(x,y)$ at the base points $\mathbf{x}_i$. Correspondingly, their reciprocal counterparts $\phi_i^{void}(\xi,\eta)$ tangent to $\phi(\xi,\eta)$ at $\xi_i$. The vertex $\mathbf{x}_v$ meets the *i*-conical condition when it corresponds to a polygon having a circumscribed circle like the green circle.

We have located one base point when the other three base points are given. In regions with no umbilical point, we can drive a quadrilateral mesh with m-by-n base points when m+n−1 base points are given.

## 4 Boundary conditions

Earlier, we discussed the equilibrium within a domain. At the boundary, the material may not always have sufficient bounding traction to develop normal or shear stresses. To establish a local coordinate system following the boundary, let $\mathbf{n}=(n_x,n_y)$ denote the normal direction and $\mathbf{t}=(t_x,t_y)=(-n_y,n_x)$ the tangential direction. The transformation of the stress tensor can be given as:

$$\begin{bmatrix} \sigma_{nn} & \sigma_{nt} \\ \sigma_{nt} & \sigma_{tt} \end{bmatrix} = \begin{bmatrix} n_x & n_y \\ -n_y & n_x \end{bmatrix} \begin{bmatrix} \sigma_{xx} & \sigma_{xy} \\ \sigma_{xy} & \sigma_{yy} \end{bmatrix} \begin{bmatrix} n_x & -n_y \\ n_y & n_x \end{bmatrix}.$$

We can classify the boundaries into four types based on their traction (Csonka 1987; Sadd 2009) (**fig. 10**):

- Free edges: No reactions in normal and shear directions ($\sigma_{nn}=0$ and $\sigma_{nt}=0$).
- Reinforced edges: Reactions in tension and compression but pliable in bending (shear resistance to the material but no normal stress) ($\sigma_{nn}=0$).
- Sliding supports: No reactions in tangential direction, but reactions in normal direction ($\sigma_{nt}=0$).
- Fixed supports. Material adequately attached to the foundation.

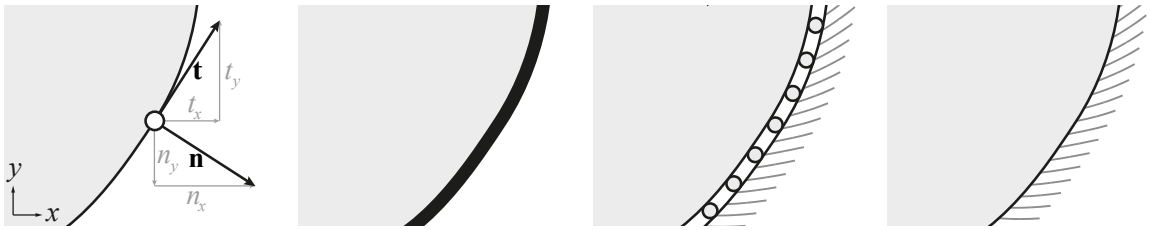


**Figure 10:** Types of boundary conditions and their schematic figure representation.

## 5 Beams under self-weight

In linear elasticity, when compatibility is considered and the body forces are zero or uniform, the Airy stress function should follow the bi-harmonic equation (Sadd 2009):

$$\frac{\partial^4 F}{\partial x^4} + 2\frac{\partial^4 F}{\partial x^2 \partial y^2} + \frac{\partial^4 F}{\partial y^4} = 0. \tag{20}$$

A solution to **eq. (20)** for a simply supported beam with reinforced ends can be expressed as Sadd (2009)

$$F(x,y) = -\frac{2R}{L}\left[\left(x^2 - \frac{L^2}{4}\right)\frac{y^2}{H^2}\left(\frac{y}{H} - \frac{3}{2}\right) - \frac{y^2}{5}\left(\frac{y}{H} - \frac{1}{2}\right)\left(\frac{y}{H} - 1\right)^2\right], \tag{21}$$

in which $R$ denotes the reaction force at one of the supports, $L$ the length of the beam, and $H$ the depth.

We can interpret the stress function as body forces being zero and all the loads acting on top. Subsequently, we can discretise the stress function into a planar *i*-circular mesh. The mesh highlights the principal curvatures of the graph (Bobenko and Suris 2007; Pottmann and Liu 2007), or the principal stresses of the beam, as **fig. 11a** shows. The stress $\sigma_{yy}$ equals $2R/L$ at the top and gradually becomes $0$ at the bottom of the beam.

We can also interpret the same stress function **eq. (21)** when body forces are

$$p_x = 0, \text{ and } p_y = \frac{2R}{LH}.$$

In this case, the beam is loaded by its self-weight and there is no external load at the top. Accordingly, We shall discretise the stress function into a non-planar *i*-circular mesh, as **fig. 11b** shows. In this case, the stress $\sigma_{yy}$ equals $0$ at the top, middle, and the bottom of the beam.

These two cases follow the same governing equation and are represented by the same smooth stress function. But after we discretise them, the planar and curved faces develop the crease angles differently at the edges and therefore reveal different stresses in the bars.

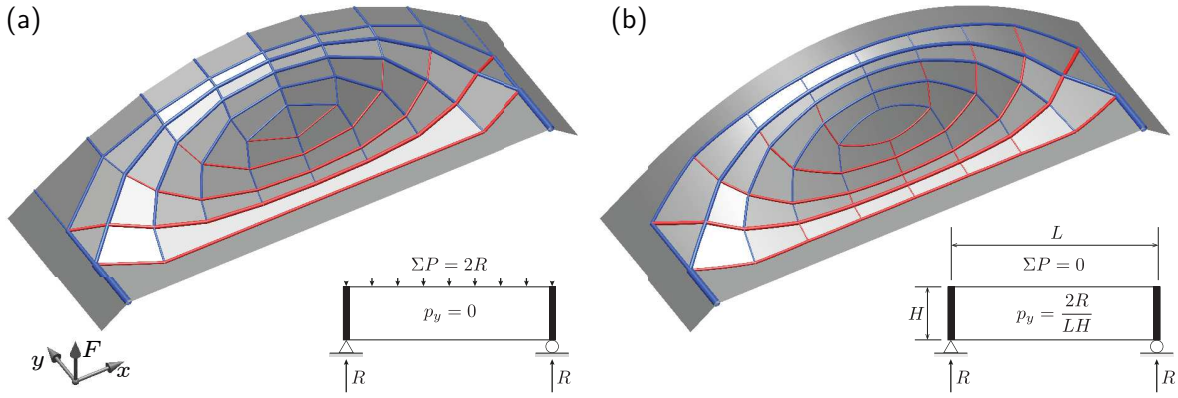


**Figure 11:** Discretised Airy stress functions of simply-supported beams. The beam in (**a**) is externally loaded on top without body forces while the beam in (**b**) is loaded by its own weight. The diameters of the bars are proportional to their axial forces. Blue bars are in compression and red bars in tension.

# 6 Conclusion

We have developed a method to incorporate body forces in the discretised Airy stress function of a structure. One discretised Airy stress function can contain information from three functions: the integrals of body forces $\int p_x\,dx$, $\int p_y\,dy$, and the smooth Airy stress function $F(x, y)$ in one geometry. The integrals of body forces are discretised into step-wise functions which inform the curvatures of the discretised Airy stress function. In the discretised Airy stress functions, the curved faces represent voids and curved creases represent stressed bars. The curvatures on the curved faces represent in-active stresses. These stresses become active on the borders between faces with different curvatures. The reciprocal relationship between a discrete Airy stress function and its reciprocal diagram is reintroduced, where vertices map to planar faces, straight edges to other straight edges, and planar faces to vertices. To include body forces, new entities are introduced into this reciprocal relationship, namely: curved edges, developable surfaces and doubly-curved surfaces that respectively map to developable surfaces, curved edges, and doubly curved surfaces. By applying non-planar *i*-circular and *i*-conical meshes, the edges of these quad-dominant meshes can highlight the principal stresses.

Smooth Airy stress functions may not be easy to read. By discretisation, the distributed stress tensors concentrate into edges of principal wireframes that are easily understood. By introducing body forces into the stress function, the influence of self-weight can be incorporated, and with that be visualised.

The proposed method currently only focuses on statics and compatibility, and does not yet include large deformations. Regarding validating whether this visualisation technique actually generates more perceptible results, experiments shall be made.

## References

Airy, G. B. (1863). On the Strains in the Interior of Beams. *Philosophical Transactions of the Royal Society of London 153*, 49–79.

Arfken, G. B., H. J. Weber, and F. E. Harris (2013). *Mathematical methods for physicists* (Seventh Edition ed.). Boston: Academic Press.

Block, P. and J. Ochsendorf (2007). Thrust network analysis: A new methodology for three-dimensional equilibrium. *Journal of the International Association for Shell and Spatial Structures 48*(155), 167–173.

Bobenko, A. I. and Y. B. Suris (2007). On organizing principles of discrete differential geometry. Geometry of spheres. *Russian Mathematical Surveys 62*(1), 1–43.

Chen, B.-Y., S. Decu, and L. Verstraelen (2014). Notes on isotropic geometry of production models. *Kragujevac Journal of Mathematics 38*(1), 23–33.

Cremona, L. (1875). *Elements of projective geometry*. Clarendon Press.

Cremona, L. (1890). *Graphical Statics: Two Treatises on the Graphical Calculus and Reciprocal Figures in Graphical Statics*. Oxford: Clarendon Press.

Csonka, P. (1987). *Theory and practice of membrane shells*. Düsseldorf: VDI Verlag.

Culmann, C. (1866). *Die graphische statik*. Zürich: Meyer & Zeller.

Fraternali, F., M. Angelillo, and A. Fortunato (2002). A lumped stress method for plane elastic problems and the discrete-continuum approximation. *International Journal of Solids and Structures 39*(25), 6211–6240.

Heyman, J. (1977). *Equilibrium of shell structures*. Oxford: Oxford University Press.

Liu, Y., H. Pottmann, J. Wallner, Y.-L. Yang, and W. Wang (2006). Geometric modeling with conical meshes and developable surfaces. In *ACM SIGGRAPH 2006 Papers*, New York, pp. 681–689. Association for Computing Machinery.

Maxwell, C. (1864). On reciprocal figures and diagrams of forces. *The London,*

*Edinburgh, and Dublin Philosophical Magazine and Journal of Science 27*(182), 250–261.

Maxwell, C. (1868). On Reciprocal Diagrams in Space and their relation to Airy's Function of Stress. *Proceedings of the London Mathematical Society 1*(1), 58–63.

Maxwell, C. (1870). On reciprocal figures, frames, and diagrams of forces. *Earth and Environmental Science Transactions of the Royal Society of Edinburgh 26*(1), 1–40.

McKitterick, D. (1995). *The Making of the Wren Library: Trinity College, Cambridge*. Cambridge University Press.

Porteous, I. R. (2001). *Geometric differentiation: for the intelligence of curves and surfaces*. Cambridge University Press.

Pottmann, H. and Y. Liu (2007). Discrete surfaces in isotropic geometry. In *IMA Int. Conference on Mathematics of Surfaces*, Berlin, pp. 341–363. Springer.

Pottmann, H. and K. Opitz (1994). Curvature analysis and visualization for functions defined on euclidean spaces or surfaces. *Computer aided geometric design 11*(6), 655–674.

Pottmann, H. and J. Wallner (2008). The focal geometry of circular and conical meshes. *Advances in Computational Mathematics 29*(3), 249–268.

Sadd, M. H. (2009). *Elasticity: Theory, Applications, and Numerics* (2 ed.). Burlington: Academic Press.

Sokolnikoff, I. S. (1956). *Mathematical theory of elasticity*. New York: McGraw-Hill.

Varignon, P. (1725). *Nouvelle Mecanique Ou Statique: Dont Le Projet Fut Donné En M. DC. LXXXVII*. Jombert.

Zadravec, M., A. Schiftner, and J. Wallner (2010). Designing quad-dominant meshes with planar faces. In *Computer Graphics Forum*, Volume 29, pp. 1671–1679. Wiley Online Library.